Article:

O'Keeffe, H., Rehman, F.J., Holmes, T.D. et al. (3 more authors) (2025) Targeted-waveform optimisation for ozonising dielectric barrier discharge reactors. Ozone: Science & Engineering. ISSN 0191-9512

https://doi.org/10.1080/01919512.2025.2453579

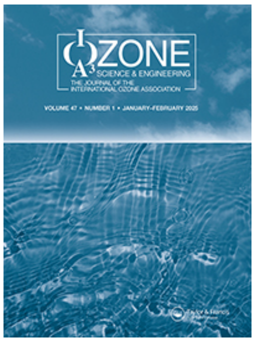

Ozone: Science & Engineering
The Journal of the International Ozone Association

ISSN: (Print) (Online) Journal homepage: www.tandfonline.com/journals/bose20

Targeted-Waveform Optimisation for Ozonising Dielectric Barrier Discharge Reactors

Henry O'Keeffe, Fahad J Rehman, Thomas D Holmes, Jonathan N Davidson, Martin P Foster & William B.J. Zimmerman

To cite this article: Henry O'Keeffe, Fahad J Rehman, Thomas D Holmes, Jonathan N Davidson, Martin P Foster & William B.J. Zimmerman (24 Jan 2025): Targeted-Waveform Optimisation for Ozonising Dielectric Barrier Discharge Reactors, Ozone: Science & Engineering, DOI: 10.1080/01919512.2025.2453579

To link to this article: https://doi.org/10.1080/01919512.2025.2453579

Published online: 24 Jan 2025.

OZONE: SCIENCE & ENGINEERING
https://doi.org/10.1080/01919512.2025.2453579

Targeted-Waveform Optimisation for Ozonising Dielectric Barrier Discharge Reactors

Henry O'Keeffe[a], Fahad J Rehman[b], Thomas D Holmes[c], Jonathan N Davidson[a], Martin P Foster[a], and William B. J. Zimmerman[c]

[a]School of Electrical and Electronic Engineering, University of Sheffield, Sheffield, UK; [b]Department of Chemical Engineering, COMSATS University Islamabad, Pakistan; [c]School of Chemical, Material and Biological Engineering, University of Sheffield, Sheffield, UK

ABSTRACT
In this work, a method for maximizing the efficacy of ozone production by dielectric barrier discharge (DBD) is presented. By developing an optimiser-based hardware-in-the-loop system, the effects of varying input waveform parameters and the flowrate of the input gas on the reactor conditions could be explored with greater fidelity than in previous literature. The waveform used is biharmonic, consisting of the sum of two sine waves and allowing a greater number of explorable parameters. The performance of the reactor, evaluated using the parametric sweep technique, is compared to that of a hybrid optimiser combining particle swarm optimisation and pattern search. Two metrics were targeted: ozone concentration-to-power ratio (ppm/W) and ozone quantity for a given energy (g/kWh). Thus, the characteristics of the input voltage waveform and flowrate were adjusted to target high ozone generation efficacy for the reactor used in the experiment. Results show that the optimiser achieves 343 ppm/W compared to 170 ppm/W for the parametric sweep, using a similar number of measurements.

ARTICLE HISTORY
Received 24 October 2024
Accepted 3 January 2025

KEYWORDS
Dielectric Barrier Discharge; Optimisation; Ozoniser

Introduction

Dielectric barrier discharge (DBD) is a type of electrical discharge generating non-thermal or "cold" plasma. It finds widespread use in the generation of ozone, where it is more efficient than other techniques such as oxygen photolysis by ultra-violet radiation (Nassour et al. 2016). Specific applications include the sterilisation of equipment (Kogelschatz 2003), anti-microbial food treatment (Obileke et al. 2022), and the catalysis of reactions in chemical engineering (Zeng et al. 2023).

DBD requires a high voltage alternating current (HV AC) power supply connected to two or more electrodes with at least one dielectric barrier and one reaction gap between them (Kogelschatz 2003). An example is shown in Figure 1.

As the voltage applied to the electrodes varies, a charge builds on the dielectric barrier until the localized voltage across the reaction gap exceeds the dielectric strength of the gas in the gap. The subsequent breakdown is limited by the charge in the dielectric, confining the discharge to a narrow region known as a streamer and limiting the energy in the plasma.

Several metrics are used to measure the efficacy (effectiveness) of ozone generation. The most common is a ratio of a quantity of ozone generated and the energy used to produce the ozone, e.g., g/kWh, usually measured at the input of the reactor,

$$\eta_q = \frac{m_{O_3}}{E} \quad [1]$$

where η_q is quantitative efficacy, m_{O_3} is the mass of ozone produced and E is the energy consumed by the reactor. Another useful metric is the ratio of the ozone concentration to power which is measured in units of ppm/W and represented by the symbol η_c,

$$\eta_c = \frac{O_3}{P} \quad [2]$$

where O_3 is the concentration of ozone and P is the power used by the reactor.

Usually, η_c is used when the flowrate is kept constant and is therefore proportional to η_q. If a chemical reaction is limited by the concentration of ozone, keeping the gas/liquid interface area constant, η_c might be more useful than η_q.

The AC waveform used to power DBD reactors is usually sinusoidal, and the voltage is necessarily high

CONTACT Henry O'Keeffe h.okeeffe@sheffield.ac.uk School of Electrical and Electronic Engineering, University of Sheffield, Sir Frederick Mappin Building, Mappin Street, Sheffield S1 3JD, UK

This article has been corrected with minor changes. These changes do not impact the academic content of the article

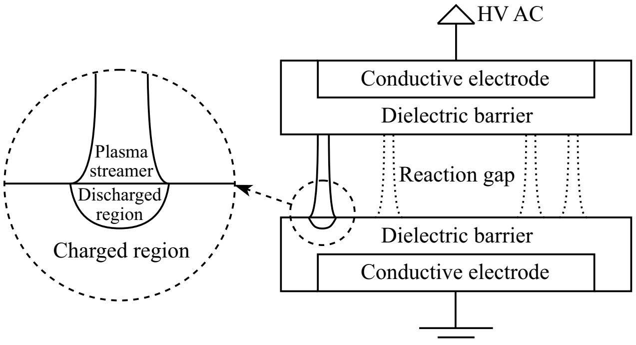

Figure 1. Cross-section of a dielectric barrier discharge (DBD) reactor.

enough to cause the gas in the reaction gap (Figure 1) to undergo dielectric breakdown, usually >1 kV. The frequency varies depending on the reactor and its application. A higher frequency allows for greater plasma formation as the number of discharges per period is independent of frequency; the higher the frequency, the higher the number of periods per second, and the more discharges occur per second (Kogelschatz 2003). This usually results in greater ozone production at higher frequencies, at the cost of a more complex power supply (PSU) and increased input power. For example, medium power reactors (<100 kW) may use a frequency in kHz (Alonso et al. 2005), or even MHz (Koo, Cho and Lee 2008) due to the reduction in size and weight of high-frequency PSUs compared to line frequency PSUs. A large (>100 kW) reactor for wastewater treatment might operate at line frequency (50/60 Hz) due to the ease of obtaining high voltage directly from the grid, although even in these larger installations, PSUs operating at higher frequencies have become common (Kogelschatz 1988).

For radio frequency, sub-atmospheric-pressure plasmas, researchers have been able to adjust the waveform by altering the harmonic content to achieve controllable direct-current-self-bias and control the location of the high-intensity plasma. Heil et al. (2008), present this technique and provide a theoretical model derivation and numerical simulation. The more recent work done by Bruneau et al. (2014) focuses on the effects of the time-domain waveshape on the plasma in the spatio-temporal domain. In the work done by Derzsi et al. (2017), this technique is applied to oxygen plasma, and the effects of different fundamental frequencies are also explored. The effect of the waveform on the energy efficiency of generating certain chemical species is investigated by Korolov et al. (2021).

There has also been research on the effects of waveform on atmospheric DBD plasmas: Seri et al. (2019) explore the effect of input waveform on ozone production using an indigo probe and Zhang et al. (2019) change the flowrate of the input gas and the duty cycle of an amplitude modulated input voltage of a DBD reactor to explore the effect on efficacy.

To thoroughly explore the effects of waveform and flowrate on DBD ozoniser efficacy and determine the most efficacious parameter-set, this work employs a hybrid global optimiser to adjust the input parameters.

This technique has been used outside plasma science to alter the voltage waveform to obtain some desirable outcome. For example, in Bhowmick et al. (2024), a gate-drive waveform is adjusted to achieve high efficiency in an inverter for solar power by way of a global optimiser.

Global optimisation is a process of finding the best solution to a problem, or a solution close to the best, subject to certain constraints. In this work, optimisation is used to find waveform parameters and a flowrate that maximizes reactor efficacy. The two optimisation techniques used here are particle swarm optimization (PSO) (Kennedy and Eberhart 1995) and pattern search (PS) (Hooke and Jeeves 1961).

PSO is an optimisation algorithm inspired by the social behavior of birds. In PSO, a "swarm" of particles move through the search-space and interact with each other, where each particle represents a vector of variables providing a potential solution to the problem. The algorithm iteratively updates the position of particles within the search-space based on the optimum solution found by that particle and the global best solution, causing the particles to tend toward better solutions over several iterations. PSO has demonstrated good performance when operating on problems with multiple variables.

PS is another global optimisation technique that uses a systematic approach to explore the parameter space around a given initial point. From a given starting point, this technique searches along each dimension of the problem, where a dimension represents one variable. The optimiser moves through the search-space in steps dependent on the success of the previous step. This success is defined only by whether the solution at the newer point is better than the current best.

As the PSO is seeded with random particle locations covering the valid search-space, this allows the optimiser to cover a large area, helping to ensure that a global minimum is found. The PS technique, however, starts with a given starting point and iteratively moves toward the optimum solution, thoroughly covering the parameter space, but making it more susceptible to becoming stuck in local minima.

To combine the advantages of each optimisation algorithm, a hybrid approach is used in this work where PSO is used to find a reasonable starting point for PS to refine.

In this paper, a DBD plasma reactor hardware-in-the-loop system is embedded within an optimisation routine to determine the most efficacious parameter set. The investigation focuses on a biharmonic waveform with tuneable amplitude and phase relationships of the fundamental and second harmonics with the intention of determining the 'optimal' parameter set. It is shown that the use of an optimiser allows a higher efficacy to be found than a parametric sweep, whilst performing a similar number of tests.

DBD waveform

The biharmonic waveform for the reactor input voltage (V_R) consists of a first (fundamental) and second harmonic, termed V_{R1} and V_{R2}, respectively. The reactor voltage, V_R, is

$$V_R = \sqrt{V_{R1}^2 + V_{R2}^2} \quad [3]$$

All voltage amplitudes in this work are root-mean-squared (RMS) values. These parameters were chosen to give the waveform a wide range of possible waveshapes, whilst being easy to generate. The phase angle of the second harmonic with respect to the first is also a tuneable parameter and is represented by θ. The fundamental frequency of this waveform is kept constant.

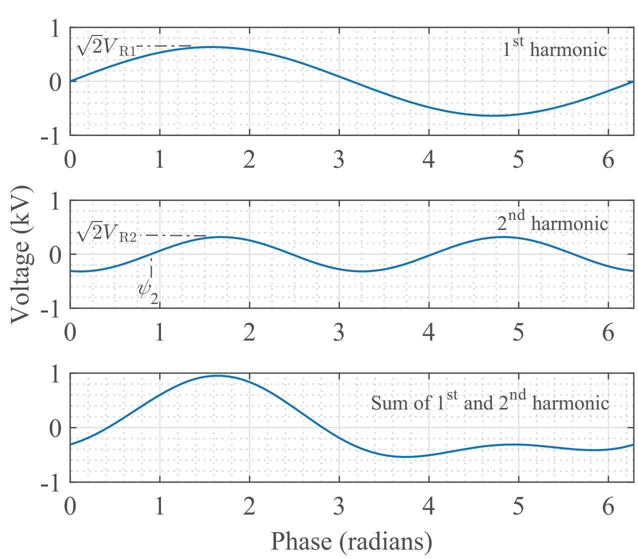

Figure 2. Biharmonic waveform decomposition showing the first and second harmonics and their sum.

The proposed system waveform allows V_{R1}, V_{R2} and θ to be varied independently. These parameters can be seen in the time domain waveforms shown in Figure 2.

Experimental materials and methods

To test how the optimisers can be used to adjust the operating conditions of a reactor to improve performance, three experiments were conducted for each of the three targeting methods.

Experiment 1 – parametric sweep: variation of four parameters; flowrate (F_A), V_{R1}, V_{R2} and θ, with linearly spaced test points for each parameter, resulting in 256 tests.

Experiment 2 – PSO for concentration efficacy: using the Matlab Optimization Toolbox with a swarm size of 20 particles and a maximum of six iterations including the starting point. The optimiser was allowed to vary the four parameters to maximize the reactor output concentration efficacy, η_c, in ppm/W. The most optimal solution was then given as the starting point to a PS optimiser which ran for a further 150 tests, for 270 tests in total.

Experiment 3 – PSO for ozone quantity: using the same optimiser as experiment 2 but maximizing ozone quantity, η_q in g/kWh, rather than η_c in ppm/W.

The fundamental frequency of the waveform was kept constant at 10 kHz for all experiments to limit the number of parameters that are to be tested. The amplitude of each harmonic was limited to approximately 3.2 kV_{RMS}, subject to further limitation by the HV amplifier. Flowrate, F_A, ranged from 0.1 to 10 L/min (liters per minute), and phase was varied through 360°.

For all three experiments, and for each unique set of variables, two sets of data were obtained: A steady-state ozone reading from five consecutive measurements averaged over a 10 s period and an oscillogram of the electrical waveforms.

The Lissajous method (Peeters and Butterworth 2018) was used to calculate the reactor power due to its superior accuracy compared to methods using direct current measurement (Homola et al. 2020). This method uses a series-connected current sense capacitor, C_S, to accumulate charge. The reactor average power, P_{av}, can then be obtained with

$$P_{av} = \frac{C_S}{T_{av}} \int_{t=0}^{T_{av}} V_R(t) \mathrm{d}V_{CS}(t) \quad [4]$$

The experimental setup used is shown in Figure 3 and the equipment used can be found in Table 1.

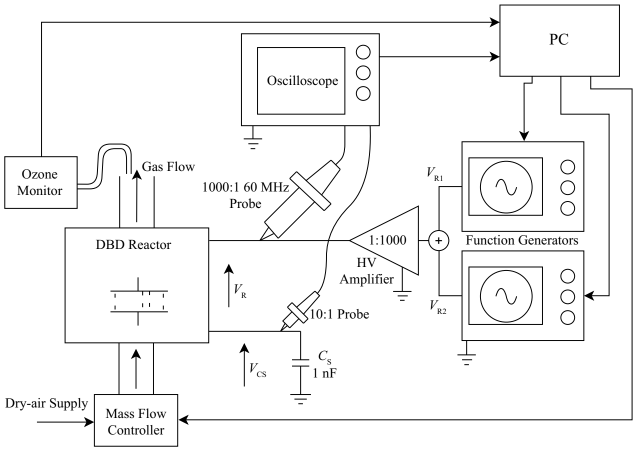

Figure 3. Experimental setup diagram.

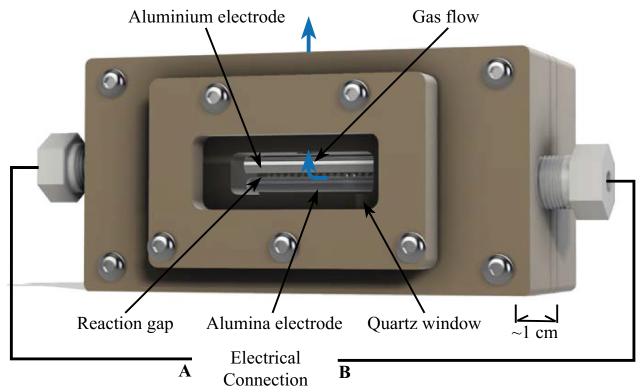

Figure 4. Annotated 3D model of the DBD reactor.

The reactor used in these experiments is asymmetrical with a pair of 3 mm diameter cylindrical electrodes, one alumina (aluminum oxide) and one aluminum. The reaction gas flows between the electrodes, separated by a reaction gap of approximately 0.25 mm. The active length of the electrodes is 20 mm, and the alumina dielectric thickness is 0.675 mm. The reactor can be operated with an input voltage of up to 5 kV_{RMS} when air is used as the reaction gas feedstock at a flowrate of up to 10 L/min. The main body of the reactor is constructed from PEEK plastic with a quartz window on the front. The design of the reactor can be seen in Figure 4. The gas enters the rear of the reactor, flows through the reaction gap as indicated by the blue arrow and exits through the top.

The reactor is driven by an HV amplifier, the input signal of which is the sum of waveforms from the two synchronized waveform generators, one operating at the first harmonic (10 kHz) and the other at the second harmonic (20 kHz). An oscilloscope is used to monitor and record the voltage on the input of the reactor and the current-sense capacitor via an HV probe and 10:1 voltage probe, respectively. An ozone monitor records the concentration of ozone in the gas flow on the output of the reactor, whilst a mass flow controller (MFC) controls the dry air input to the reactor. A PC controls the MFC and the waveform generators whilst capturing data from the oscilloscope and ozone monitor (Table 1).

Table 1. Experimental apparatus.

Ozone monitor	2B Technologies 106-MH
Oscilloscope	Picoscope 6404E
High voltage probe	Tektronix P6015A
Waveform generators	RS RSDG830
HV amplifier	Trek 10/410 A-HS
Mass flow controller	Bronkhorst F-201CV-20K-AAD-22-V

Experimental results

Figure 5 shows the reactor input power against the four controlled parameters. For Figures 5–7 and 9, the harmonic ratio (V_{R2}/V_R), second harmonic phase (θ) and flowrate (F_A) are the horizontal axes of the three sub-plots, whilst the reactor voltage (V_{R2}) is the vertical axis. In these figures, the experimental data for all three experiments are shown on the same plots, giving a total of 796 datapoints. The colour represents the highest datapoint in each bin, as other variables not plotted on each sub-figure cause significant variation between datapoints. This variation is explored in other sub-figures, where the relevant variable forms one of the axes.

The positive correlation of power and voltage shown in Figure 5(a) is evident, as expected from (Ponce et al. 2004) for waveforms with frequencies in the tens of kHz.

It can also be seen that the second harmonic voltage results in a greater power in the reactor than a first harmonic of the same voltage. This is also in accordance with the literature, as power should be approximately proportional to frequency (Kogelschatz 2003).

Reactor power vs. θ and V_R shown in Figure 5(b) indicates higher reactor power around $\theta = 0°$ and $\theta = 180°$ compared to $\theta = 90°$ and $\theta = 270°$.

Figure 5(c) shows the effects of flowrate and reactor voltage on reactor power. A weak negative trend is seen, where flowrate and power have an inverse relationship;

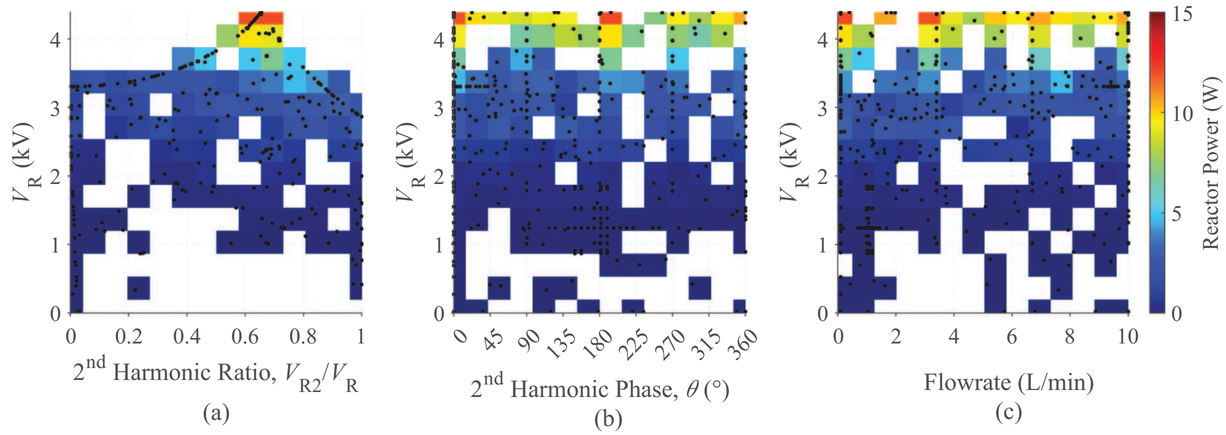

Figure 5. Reactor power with reactor voltage and the three controlled parameters combining the three experiments. Dots represent the experiment datapoints, the colour represents the highest datapoint in each bin.

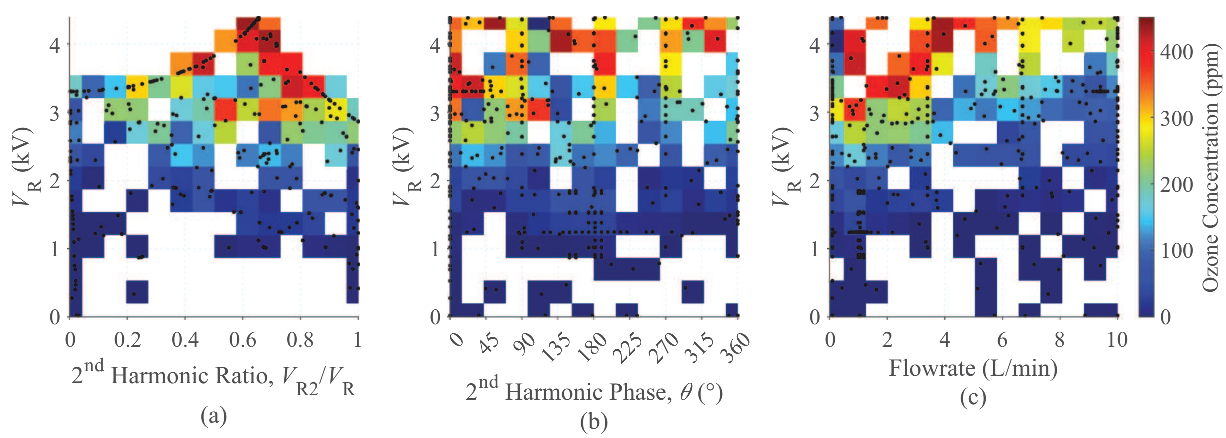

Figure 6. Ozone concentration with reactor voltage and the three controlled parameters combining the three experiments. Dots represent the experiment datapoints, the colour represents the highest datapoint in each bin.

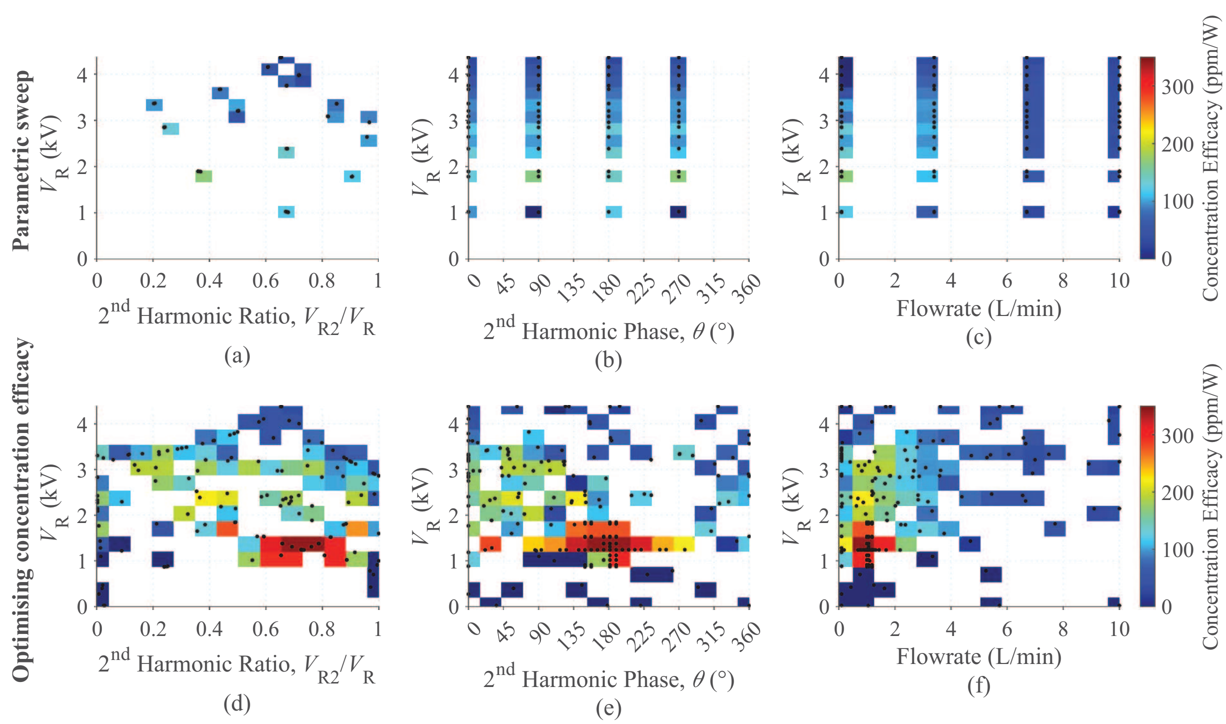

Figure 7. Ozone concentration efficacy, η_c (ppm/w) with reactor voltage and the three controlled parameters the parametric sweep and concentration efficacy optimisation. Dots represent experiment datapoints, the colour represents the highest datapoint in each bin.

with V_R approximately constant at 4400 V_{RMS}, the reactor power decreases from 11.9 to 10.5 W when flowrate is increased from 0.1 to 10 L/min. This could be due to the increased flow increasing the pressure in the reactor slightly, resulting in an increase in the breakdown voltage of the air feedstock (seen with dry air in (Fan et al. 2018)) and reducing the number of discharges per second.

The effects of the second harmonic, V_{R2}, on the ozone concentration at the output of the reactor can be seen in Figure 6(a). This graph shows the same trend as Figure 5(a), suggesting that the ozone concentration and reactor power are positively correlated. In this figure, however, there are datapoints that do not fit this trend, the orange square at ($V_{R2}/V_R = 0.5$, $V_R = 3$ kV) for example, where ozone concentration is higher than might be expected from Figure 5.

These outliers are due to the variations in the other two parameters; Figure 6(b) shows how the ozone concentration varies with second harmonic phase angle and shows a similar trend to the power in Figure 5(b), with more outliers, as the ozone concentration is heavily dependent on the flowrate, as seen in Figure 6(c).

The flow of the feedstock helps remove heat from the reactor and, as the decomposition of ozone has a strong positive correlation with temperature (Itoh, Taguchi and Suzuki 2020), very low flowrates (<1 L/min) cause a sharp decrease in ozone concentration, as seen in Figure 6(c). Outside this region, ozone concentration decreases with flowrate as the plasma produces a similar amount of ozone, but it becomes diluted with more air infeed. This relationship is not linear, however, with the ozone concentration only decreasing by approximately a factor of 2 at 10 L/min compared to the concentration at 2 L/min. This is perhaps due to the increased cooling reducing the decomposition of ozone (Itoh, Taguchi and Suzuki 2020) at higher flowrates.

Figure 7(a-d) show how the concentration efficacy varies with the harmonic ratio for each of the three experiments. A comparison of these three subplots illustrates the effectiveness of the optimisation algorithm targeting this metric. A cluster of datapoints in the high-efficacy region around ($V_{R2}/V_R = 0.75$, $V_R = 1.2$ kV) in Figure 7(d) represent the final iterations of the optimisation algorithm, as it converges to the optimal solution.

The voltages chosen by the optimiser result in V_R reaching just above the plasma ignition threshold and correspond to an ozone concentration of 10 ppm.

Figure 7(e) shows the optimiser targeting concentration efficacy converging on a small region of high efficacy around ($\theta = 180°$, $V_R = 1.2$ kV_{RMS}).

A region of higher concentration efficacy is also shown in Figure 7(f). A flowrate of ~1.2 L/min has been identified by the optimisation algorithm as having the highest efficacy, and refinement attempts around this flowrate in the parameter-space show an area of high concentration efficacy between about 0.7 and 1.5 L/min.

Taken together, Figure 7(d-f) clearly show how the optimiser explores the search space and converges on the optimum solution, which could be missed with a simple parametric sweep (Figure 7(a-c)). The optimiser found an operating point at ($V_{R2}/V_R = 0.75$, $\theta = 180°$, $F_A = 1.2$ L/min, $V_R = 1.2$ kV) with a maximum concentration efficacy of 343 ppm/W compared to 170 ppm/W obtained from the parametric sweep.

The approach taken by the optimiser is illustrated in Figure 8. Figure 8(a) shows the particle swarm optimiser

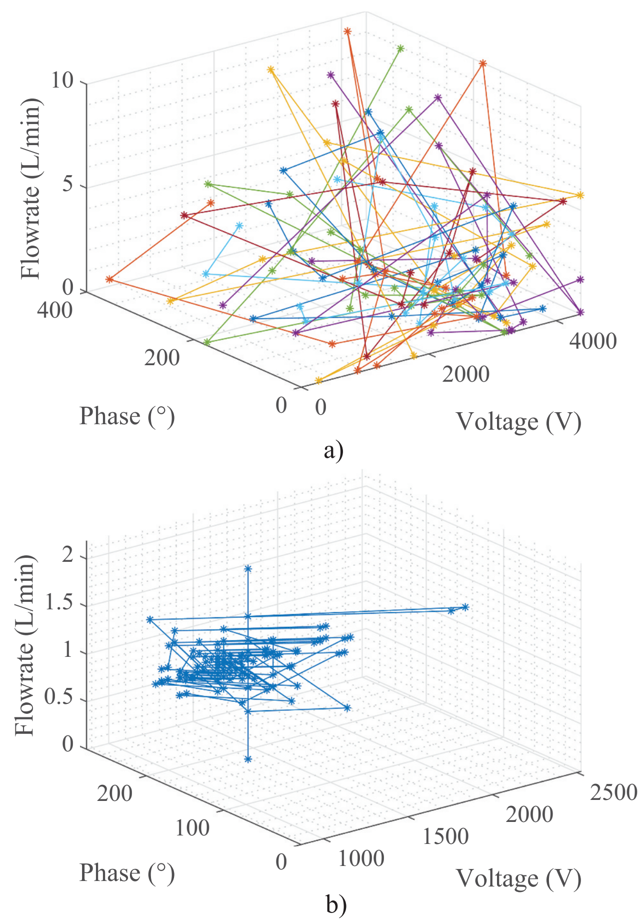

Figure 8. (a) Particle swarm optimisation iteration path for the concentration efficacy optimisation (one colour per particle), (b) Pattern search iteration path. Both plots omit the ratio of the second harmonic, although this was optimised.

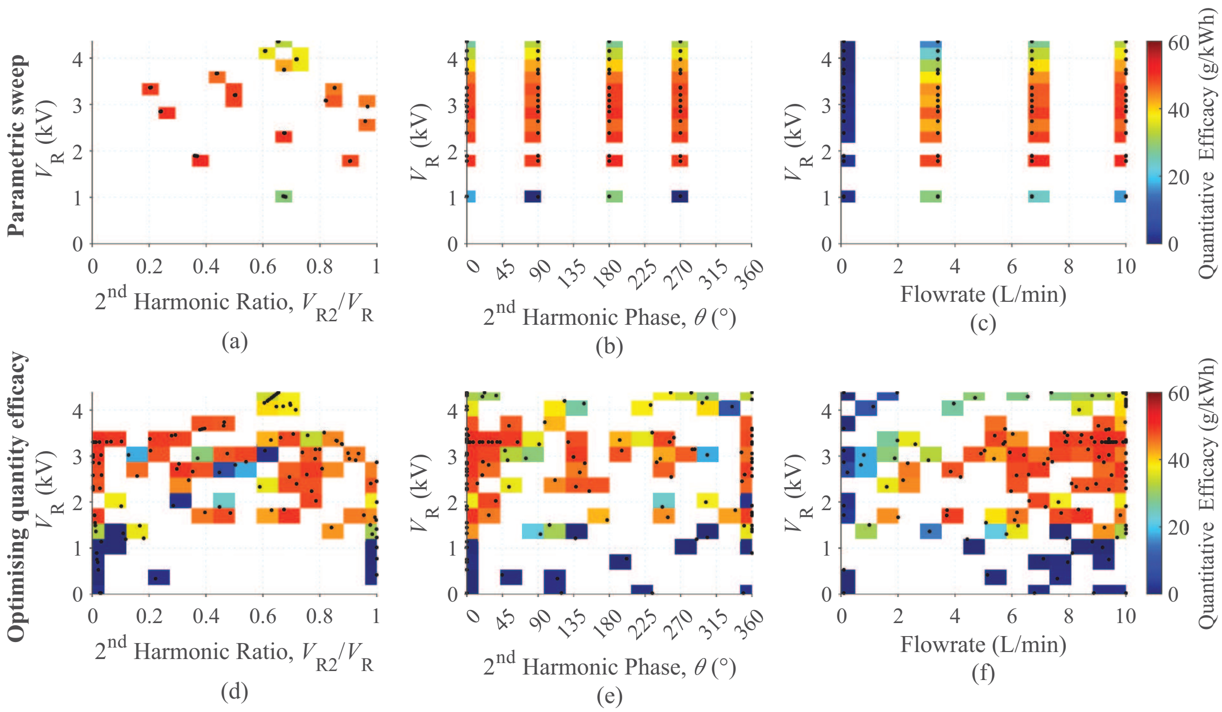

Figure 9. Ozone quantitative efficacy, η_q (g/kWh) with reactor voltage and the three controlled parameters for the parametric sweep and quantity efficacy optimisation. Dots represent experiment datapoints, the colour represents the highest datapoint in each bin.

producing 20 independent paths of five steps each to explore the parameter-space. The best of these particles then seeds the pattern search optimiser, as shown in Figure 8(b). This optimiser takes 150 steps to converge on a local minimum which, by virtue of the particle swarm optimisation, should be the global minimum.

Figure 9(a,d) show the effect of the harmonic ratio on quantitative efficacy. Efficacy is zero where the reactor voltage is lower than the ignition threshold (V_R < 0.8 kV), as there is no plasma. It can also be seen that there is lower efficacy where V_R > 4 kV across the three subplots. Elsewhere in the plot, the quantitative efficacy is high on average, the parametric sweep in Figure 9(a) showing consistently high efficacy with a slight trend favoring a low second harmonic ratio. During the quantitative efficacy experiment shown in Figure 9(d), the optimiser converged on a point with no second harmonic (V_{R2}) content and the highest achievable for this second harmonic content, $V_R = 3.3$ kV.

No clear effect of the second harmonic phase angle, θ on the quantitative efficacy can be seen in Figure 9(b,c). When V_{R2} is close to 0, θ has little to no effect. However, the optimiser still attempts to optimise its value, resulting in redundant tests where the optimizer walks along the $V_{R2}/V_R = 0$ axis.

Figure 9(c,f) show a positive correlation between quantitative efficacy and flowrate, due to the increased cooling effect of the higher flow preventing ozone decomposition, as already discussed. A cluster of datapoints in Figure 9(f) can be seen around the optimiser's final position ($V_{R2}/V_R = 0$, $\theta = 0°$, $F_A = 9.5$ L/min, $V_R = 3.3$ kV).

Table 2 shows a summary of results. All three experiments have a similar number of tests, and therefore took a similar amount of time, approximately a minute per datapoint.

Due to the number of parameters to cover, only four datapoints on each parameter could be covered with a reasonable number of tests: $4^4 = 256$ tests. This has limited the area that could be covered by the parametric sweep.

Each of the three experiments had a similar maximum quantitative efficacy, with the optimisation intended to target this metric finding the lowest, at

Table 2. Summary of results.

Experiment	No. of tests per experiment	Maximum concentration efficacy (ppm/W)	Maximum quantitative efficacy (g/kWh)
Parametric sweep	256	169.9	50.87
Optimisation for concentration efficacy	270	343.0	52.54
Optimisation for quantitative efficacy	270	246.8	50.24

50.2 g/kWh. This may be due to the large number of datapoints already close to the optimum resulting in a lack of a clear relationship between many of the parameters and the target metric, suggesting that these parameters may have little dependence on this target metric (quantitative efficacy) for the reactor and the reaction conditions used in these experiments.

Conclusion

A hardware-in-the-loop optimisation approach for targeted waveform ozone generation was presented. The technique optimised the amplitude and phase difference of a biharmonic waveform at a fixed frequency. This was compared to a parametric sweep of equivalent complexity and shows an improvement in the identified optimum operating conditions. For the tests shown, the technique resulted in an efficacy of 343 ppm/W compared to 170 ppm/W in the parametric sweep.

These results demonstrate the promise of this hardware-in-the-loop approach for optimising chemical production by dielectric barrier discharge reactors.

Acknowledgments

The authors would also like to thank Mario Dorna and other engineers at the UoS chemical engineering workshop for their work on the design and manufacture of the reactor.

For the purpose of open access, the authors have applied the Creative Commons attribution (CC-BY) license to any author-accepted manuscript arising.

Disclosure statement

No potential conflict of interest was reported by the author(s).

Funding

This work has been financially supported by EPSRC [EP/S031421/1].

References

Alonso, J. M., J. Garcia, A. J. Calleja, J. Ribas, and J. Cardesin. 2005. "Analysis, Design, and Experimentation of a High-Voltage Power Supply for Ozone Generation Based on Current-Fed Parallel-Resonant Push-Pull Inverter." *IEEE Transactions on Industry Applications* 41 (5): 1364–72. https://doi.org/10.1109/TIA.2005.853379.

Bhowmick, S., R. Vasu, S. K. Chattopadhyay, and C. Chakraborty. 2024. "A PSO-Based Optimized Hybrid PWM Strategy for a Binary Asymmetric Cascaded H-Bridge Photovoltaic Inverter with Single PV Source per Phase." *IEEE Journal of Emerging and Selected Topics in Power Electronics* 12 (2): 1654–65. Apr. https://doi.org/10.1109/JESTPE.2023.3347643.

Bruneau, B., T. Novikova, T. Lafleur, J. P. Booth, and E. V. Johnson. 2014. "Ion Flux Asymmetry in Radiofrequency Capacitively-Coupled Plasmas Excited by Sawtooth-Like Waveforms." *Plasma Sources Science and Technology* 23 (6): 065010. Aug. https://doi.org/10.1088/0963-0252/23/6/065010.

Derzsi, A., B. Bruneau, A. R. Gibson, E. Johnson, D. O'Connell, T. Gans, J.-P. Booth, et al. 2017. "Power Coupling Mode Transitions Induced by Tailored Voltage Waveforms in Capacitive Oxygen Discharges." *Plasma Sources Science and Technology* 26 (3): 034002. Feb. https://doi.org/10.1088/1361-6595/aa56d6.

Fan, Z., H. Yan, Y. Wang, Y. Liu, H. Guo, and C. Ren. 2018. "Breakdown Characteristics of Atmospheric Dielectric Barrier Discharge in Gas Flow Condition." *Physics of Plasmas* 25 (5): 053517. May. https://doi.org/10.1063/1.5018331.

Heil, B. G., U. Czarnetzki, R. P. Brinkmann, and T. Mussenbrock. 2008. "On the Possibility of Making a Geometrically Symmetric RF-CCP Discharge Electrically Asymmetric." *Journal of Physics D: Applied Physics* 41 (16): 165202. Jul. https://doi.org/10.1088/0022-3727/41/16/165202.

Homola, T., V. Prukner, P. Hoffer, and M. Šimek. 2020. "Multi-Hollow Surface Dielectric Barrier Discharge: An Ozone Generator with Flexible Performance and Supreme Efficiency." *Plasma Sources Science and Technology* 29 (9): 95014. https://doi.org/10.1088/1361-6595/aba987.

Hooke, R., and T. A. Jeeves. 1961. ""Direct Search" Solution of Numerical and Statistical Problems." *Journal of the ACM* 8 (2): 212–29. Apr. https://doi.org/10.1145/321062.321069.

Itoh, H., M. Taguchi, and S. Suzuki. 2020. "Thermal Decomposition of Ozone at High Temperature Leading to Ozone Zero Phenomena." *Journal of Physics D: Applied Physics* 53 (18): 185206. https://doi.org/10.1088/1361-6463/ab71a9.

Kennedy, J., and R. Eberhart. 1995. "Particle Swarm Optimisation." *IEEE International Conference on Neural Networks*, Perth, Australia.

Kogelschatz, U. 1988. "Advanced Ozone Generation." In Process Technologies for Water Treatment, edited by S. Stucki, 87–118. Boston, MA: Springer US. https://doi.org/10.1007/978-1-4684-8556-1_9.

Kogelschatz, U. 2003. "Dielectric-Barrier Discharges: Their History, Discharge Physics, and Industrial Applications." *Plasma Chemistry and Plasma Processing* 23 (1): 1–46. https://doi.org/10.1023/A:1022470901385.

Koo, I. G., J. H. Cho, and W. M. Lee. 2008. "Influence of the Gas Humidity on the Uniformity of RF-Powered Atmospheric-Pressure Low-Temperature DBD Plasmas." *Plasma Processes and Polymers* 5 (2): 161–67. https://doi.org/10.1002/ppap.200700068.

Korolov, I., Z. Donkó, G. Hübner, Y. Liu, T. Mussenbrock, and J. Schulze. 2021. "Energy Efficiency of Voltage Waveform Tailoring for the Generation of Excited Species in RF Plasma Jets Operated in He/N_2 Mixtures." *Plasma Sources Science and Technology* 30 (9): 095013. Sep. https://doi.org/10.1088/1361-6595/ac1c4d.

Nassour, K., M. Brahami, S. Nemmich, N. Hammadi, N. Zouzou, and A. Tilmatine. 2016. "Comparative

Experimental Study between Surface and Volume DBD Ozone Generator." *Ozone: Science & Engineering* 38 (1): 70–76. https://doi.org/10.1080/01919512.2015.1095632.

Obileke, K., H. Onyeaka, T. Miri, O. F. Nwabor, A. Hart, Z. T. Al-Sharify, S. Al-Najjar, and C. Anumudu. 2022. "Recent Advances in Radio Frequency, Pulsed Light, and Cold Plasma Technologies for Food Safety." *Journal of Food Process Engineering* 45 (10). John Wiley & Sons, Inc, Hoboken, USA, p. n/a. https://doi.org/10.1111/jfpe.14138.

Peeters, F., and T. Butterworth. 2018. "'Electrical Diagnostics of Dielectric Barrier Discharges', in *Atmospheric Pressure Plasma - from Diagnostics to Applications*." *IntechOpen*. https://doi.org/10.5772/intechopen.80433.

Ponce, M., J. Aguilar, J. Fernandez, E. Beutelspacher, J. M. Calderon, and C. Cortes. 2004. "Linear and Non Linear Models for Ozone Generators Considering Electrodes Losses." *2004 IEEE 35th Annual Power Electronics Specialists Conference*, 810–14, Vol. 1. Piscataway, NJ. IEEE. https://doi.org/10.1109/PESC.2004.1355853.

Seri, P., A. Wright, A. Shaw, F. Iza, H. Bandulasena, C. A. Borghi, G. Neretti, et al. 2019. "Influence of the Voltage waveform's Shape and On-Time Duration on the Dissolved Ozone Produced by a DBD Bubble Reactor." *Plasma Sources Science and Technology* 28 (3): 035001. Mar. https://doi.org/10.1088/1361-6595/ab024f.

Zeng, Y., G. Chen, B. Liu, H. Zhang, and X. Tu. 2023. "Unraveling Temperature-Dependent Plasma-Catalyzed CO_2 Hydrogenation." *Industrial & Engineering Chemistry Research* 62 (46): 19629–37. Nov. https://doi.org/10.1021/acs.iecr.3c02827.

Zhang, Y., L. Wei, X. Liang, and M. Šimek. 2019. "Ozone Production in Coaxial DBD using an Amplitude-Modulated AC Power Supply in Air." *Ozone: Science & Engineering* 41 (5): 437–47. Sep. https://doi.org/10.1080/01919512.2019.1565986.